Extreme ultraviolet alignment and testing of a four-mirror ring field extreme ultraviolet optical system

Kenneth A. Goldberg,[a] Patrick Naulleau, Phillip Batson, Paul Denham, and Erik H. Anderson
Center for X-Ray Optics, Lawrence Berkeley National Laboratory, Berkeley, California 94720

Henry Chapman
Lawrence Livermore National Laboratory, Livermore, California 94550

Jeffrey Bokor[b]
EECS Department, University of California, Berkeley, California 94720

(Received 1 June 2000; accepted 23 August 2000)

Extreme ultraviolet (EUV) interferometry has been used to characterize and align a recently fabricated, 4× reduction, four-mirror, aspheric optical system designed for EUV lithography. This system is called the Engineering Test Stand Set-1 Optic. An EUV phase-shifting point diffraction interferometer constructed on an undulator beamline at the Advanced Light Source was used to perform high-accuracy wavefront measurements during several alignment iterations. For each iteration, the alignment algorithm used 35 wavefront measurements recorded across the 26-mm-wide image-side ring field. Adjustments were made to systematically reduce the root mean square wavefront error magnitude to approximately 1 nm, bringing the system to nearly diffraction-limited performance. © *2000 American Vacuum Society.* [S0734-211X(00)05106-4]

I. INTRODUCTION

A growing number of all-reflective, multilayer-coated optical systems have been fabricated for use in the development of extreme ultraviolet (EUV) lithographic technologies.[1–5] Operating near 13 nm wavelength, these systems are typically composed of multiple spherical and aspherical mirrors fabricated and aligned to operate with subnanometer system wavefront tolerances. Reflective multilayer coatings are deposited, often with a graded thickness profile, across the mirror surfaces to ensure well-controlled, high EUV reflectivity for a range of ray angles within a large field of view.

The assembly and alignment of these optical systems involves several steps. First, visible-light interferometry[6] is used during the fabrication of the individual mirrors, which are typically made from low-thermal-expansion-material substrates. EUV reflectometry[7,8] is used during the coating process to test the quality and profile of the multilayer coatings. The individual mirrors are mounted in a supporting frame and prealigned to mechanical tolerances. System-level visible-light interferometry is used to align the system and to set the positions of the conjugate planes relative to fixed sensors on the optical housing. Finally, EUV interferometry is used to verify, and if necessary, correct the alignment. EUV interferometry as a final step also serves to validate the collective performance of all the other supporting metrologies.

At-wavelength EUV metrology is essential to the development of diffraction-limited optical systems for EUV lithography. Probing the resonant reflective surfaces with EUV light at the operational wavelength reveals subtle yet important coating effects, where potential problems could otherwise be hidden. The multilayer coatings, which typically consist of 40 molybdenum–silicon bilayer pairs, have period, or *d*-spacing, thicknesses in the range of 6–7 nm.[9] Small variations in the multilayer period and/or the presence of surface contaminants can have a significant impact on the intensity and the phase of reflected EUV light, yet these effects evade simple detection with visible light.[4] At-wavelength inspection of an optical system can also be configured for *in situ* flare measurements,[10] and for the investigation of chromatic effects, including both throughput and chromatic aberrations.[11]

Where sufficient coherent EUV power is available,[12] the phase-shifting point diffraction interferometer (PS/PDI) has emerged as the design of choice for at-wavelength testing of diffraction-limited EUV optical systems. With operating wavelengths near 13 nm, angstrom-scale wavefront measurement accuracy and precision are required. The PS/PDI offers demonstrated root mean square (rms) wavefront measuring accuracy beyond $\lambda_{EUV}/300$, or 0.04 nm.[13,14]

Operating at the Advanced Light Source (ALS) synchrotron radiation facility at Lawrence Berkeley National Laboratory (LBNL). PS/PDI interferometry has been used in the measurement and alignment of several small-field EUV 10× Schwarzschild objectives.[15] Independent verification of the interferometer's accuracy and its utility in correctly predicting imaging performance has come from ongoing lithographic exposure experiments conducted at Sandia National Laboratories (SNL).[2]

A new branchline of the ALS undulator source was constructed specifically for at-wavelength testing of the projection optics for the Engineering Test Stand (ETS).[16] The ETS is now being constructed at SNL. The first of two projection optical systems is called the ''ETS Set-1 Optics,'' also pre-

[a]Electronic mail: KAGoldberg@lbl.gov
[b]Also at: Center for X-Ray Optics, Lawrence Berkeley National Laboratory, Berkeley, California 94720.

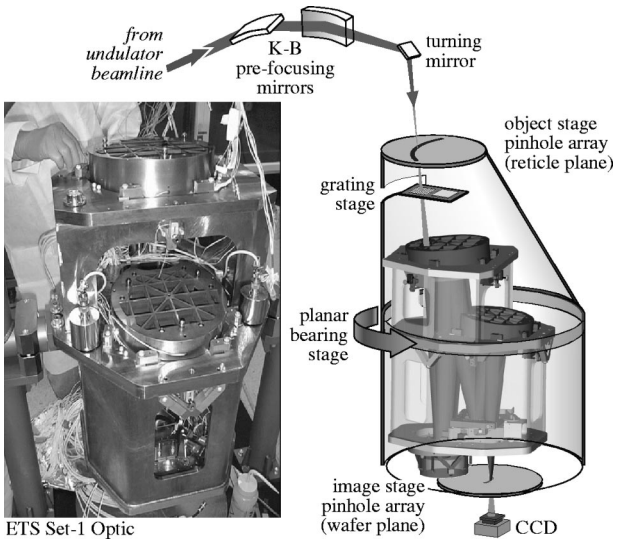

FIG. 1. (**Left**) Photograph of the four-mirror ETS Set-1 optic. (**Right**) Schematic of the experimental system showing the critical optical components of the illumination prefocusing system and the interferometer. The object and image stages rotate and translate together with the test optic; all are attached to a rigid frame mounted to a planar bearing stage within a large vacuum chamber. The grating-beamsplitter stage and the CCD camera remain fixed as the rest of the system moves.

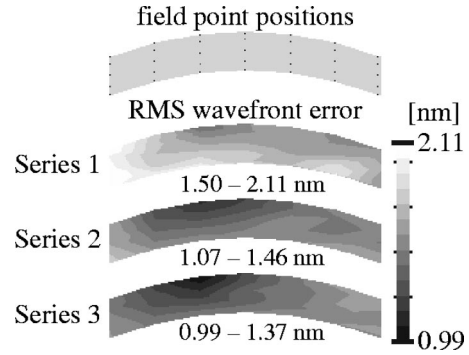

FIG. 2. The rms wavefront error magnitudes measured at 35 positions within the field of view are shown separately for each of three system measurements. Error magnitudes are based on reconstructions from the first 37 Zernike polynomial terms. Between the measurement series, the mirrors of the test optic were adjusted to reduce the field-weighted rms wavefront error. The black points in the uppermost plot show the positions at which the measurements were made. The minimum and maximum measured wavefront error magnitudes are shown below each plot.

viously, the ''Projection Optics Box.'' The system is a four-mirror ring-field EUV optical system, designed to operate at 13.4 nm wavelength with 0.1 numerical aperture (NA) and 4× demagnification.

The ETS Set-1 optic was produced by the Virtual National Laboratory in collaboration with the EUV Limited Liability Company (LLC). It was assembled at Lawrence Livermore National Laboratory and aligned initially using visible-light interferometry[16,17] before transportation to LBNL. Visible-light interferometry was performed within a vacuum chamber in a temperature-controlled clean-room environment. At LBNL the optic was installed in a similar vacuum chamber held at a matching temperature. Initial measurements provide data on the stability of the optical housing, the robustness of the system to withstand transportation, and on the relative agreement between visible-light and EUV interferometries.

II. CONFIGURATION OF THE EUV INTERFEROMETER FOR ETS SET-1 OPTICS MEASUREMENT

The PS/PDI interferometer was constructed to evaluate the system wavefront at arbitrary positions across the field of view. Measurements of the field-dependent optical performance, across the large ring-field imaging area, provide feedback for the alignment of the individual mirror elements, enabling optimal imaging quality to be achieved. A more complete description of the interferometer and its operation has been provided in prior publications.[18–20]

The PS/PDI design has only a few critical optical components. A photograph of the ETS Set-1 optic and a schematic of the interferometer configuration are shown in Fig. 1. All of the components exist in a vacuum environment with a base pressure of 10^{-7} Torr; a partial pressure of 10^{-5} Torr of oxygen gas is introduced as a preemptive contamination mitigation measure. Within the vacuum chamber, a synchrotron beam from an undulator source illuminates the object (reticle) side of the test optic from above in a manner that reproduces the way in which the optic is designed to be used. Kirkpatrick–Baez prefocusing optics and a 45° multilayer-coated turning mirror together focus the beamline radiation into a nominally 5 μm spot in the object plane of the test optic.

A small pinhole in the object (reticle) plane (the *object pinhole*) produces coherent, spherical-wave illumination of the test optic, filling the pupil of the optical system with a divergence angle significantly larger than the input NA of the system. A grating beamsplitter placed between the object pinhole and the test optic creates a series of overlapping coherent beams that are focused in the image (wafer) plane. Each of the beams from the grating acquires the aberrations of the test optic via transmission through the optical system. In the image plane where the multiple beams form separable foci displaced by several microns, a patterned, opaque and transparent mask selects two adjacent beams; all other beams are blocked. One of the two beams, the *test beam*, is passed through a relatively large open window in the mask and propagates on to reach an EUV charge coupled device (CCD) camera. The second beam is focused onto a pinhole (the *reference pinhole*) smaller than the diffraction-limited resolution of the test optic, thereby producing a spherical *reference beam*. The two beams overlap at the CCD where their interference pattern is recorded. Analysis of the interferogram reveals the path length difference between the test beam and the spherical reference, and hence contains the wavefront aberrations of the test optic.

To collect one set of wavefront data, point-by-point wavefront measurements were recorded across the ring-shaped field of view by rotating the entire optical system and the conjugate-plane stages together as one unit beneath the sta-

tionary illuminating beam. The grating is only slightly larger than the beam diameter where the beam passes through it; except for small translations associated with phase shifting, the grating position remains fixed. The CCD camera position is also fixed, facing upward. As the test optic is translated, the beam footprint on the CCD moves by several millimeters, yet the CCD is positioned close enough that the beam does not extend beyond the edges of the 1-sq-in. active area.

Similar arrays of pinholes are placed in the object plane and (with an appropriate 4× reduction in size) the image plane. The pinhole arrays are fabricated with electron beam lithography at LBNL's Nanowriter facility.[21] Wafers containing the pinhole arrays are mounted to stages that move with the optical system. With the image-plane pinholes aligned to match the conjugate positions of the object pinholes, the image-plane pinhole array need only be moved by a few microns, for fine alignment, during the measurement series. While it is true that only one object pinhole and one image pinhole are necessary to perform a measurement at a given field point, the object- and image-plane pinhole arrays were designed with a high degree of redundancy and a large number of available pinholes. A range of pinhole sizes helps to guarantee that pinholes of optimal size (once that size is determined) are available for use within each field point. The pinhole arrays also contain various alignment features that help to establish unambiguously the beam's position within the array.

To facilitate alignment of the illuminating beam through the object pinholes, the grating stage contains a photodiode that can be inserted or removed from the light path. The CCD camera provides similar feedback for light passing through pinholes on the image side.

III. PO BOX MEASUREMENT AND ALIGNMENT

Four complete sets of EUV PS/PDI measurements were performed over a six week time period. The initial measurement was made at the ambient laboratory temperature of 24.5 °C, before a thermal stabilization system was activated. The subsequent three measurements were made at 20.45 ±0.02 °C, within 0.05° of the design operating temperature of 20.5 °C. Using an alignment algorithm developed for both EUV and visible-light interferometry,[22] small mirror adjustments were made to reduce the field-weighted rms wavefront error.

The initial measurements showed that the optical system maintained its alignment very well during transportation from Livermore to Berkeley and installation in the EUV interferometer. Some of the wavefront discrepancy may be attributable to a failed micrometer used to set the longitudinal position of the object stage. In addition to distortion (which was not measured at-wavelength), longitudinal displacement of the conjugate planes can introduce wavefront astigmatism.

A. Measurement procedure

The same measurement procedure is followed at each measurement position within the field of view. Initially, the optical system and the accompanying stages are rotated and translated to bring the downward-propagating illuminating beam through an object pinhole at a desired measurement position in the field of view. Appropriate object pinholes are nominally 250 nm in diameter. The grating beamsplitter, which can be completely removed for alignment purposes, typically remains installed during the entire set of field-point measurements. The image stage is translated both laterally and longitudinally to bring one of the focused diffracted beams through an image-plane window. From there, the image stage is translated to bring an adjacent reference pinhole into the beam for interferometry. Typical reference pinhole sizes used were on the order of 80 nm in diameter.

The pinholes in both conjugate planes are arrayed in a regular pattern containing a number of nominally identical pinholes to choose from. To identify and reduce potential systematic and random errors, five or more individual wave-

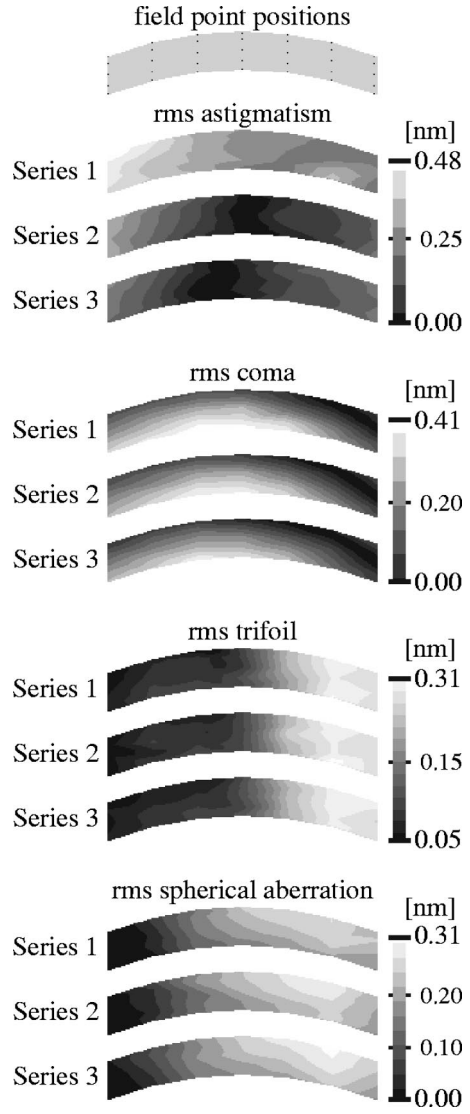

FIG. 3. The individual Zernike coefficient magnitudes of the most significant wavefront aberrations components, shown for each of the three measurement series. Notice that the alignment causes a significant reduction in astigmatism. The other aberration components are much less sensitive to small mirror tilts and displacements, and are thus largely unaffected by the alignment.

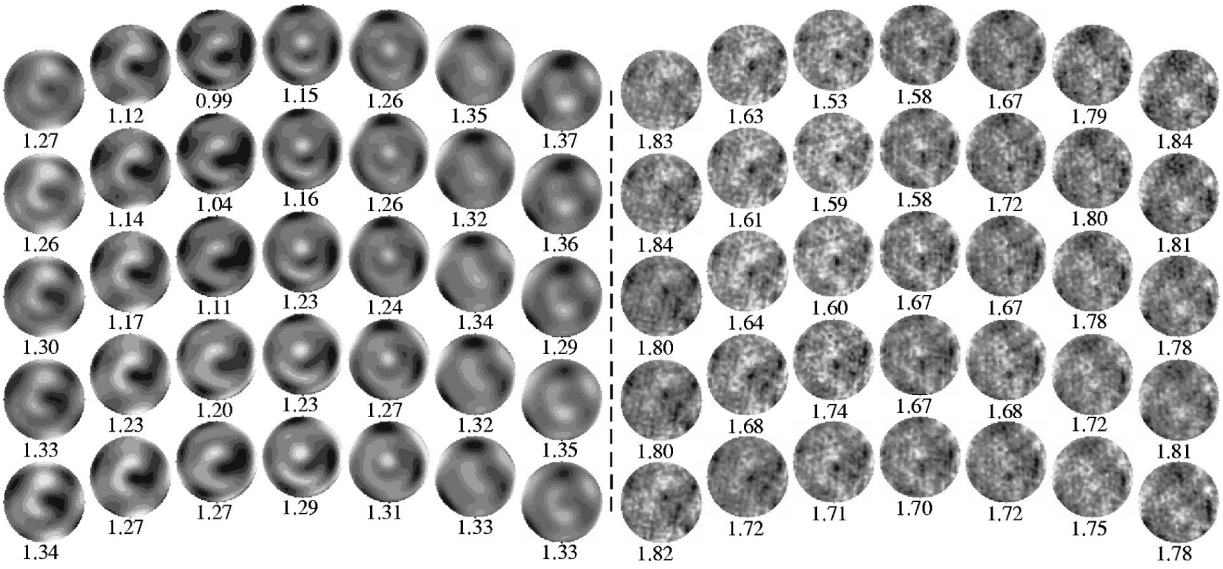

FIG. 4. Wavefront phase maps measured at 35 points across the field of view. (**Left**) Shown are reconstructions from 37 term Zernike polynomial fitting and the rms magnitude of the wavefront error in nanometers. Gray levels represent steps of 0.75 nm. (**Right**) Wavefronts and their associated rms magnitudes (in nm) are shown with higher spatial frequency content than is contained within 37 term Zernike polynomial reconstructions. Gray levels represent steps of 1.0 nm.

front measurements are typically combined to produce a single result. With each successive iteration of the system alignment procedure, a new corresponding pair of object and image pinholes was used.

Because the beam footprint rotates and translates across the fixed position of the CCD, and hence the fixed grid of pixels that define the initial measurement coordinates, it is necessary to track the motion of the projected pupil and incorporate the moving coordinate system in the wavefront analysis.

Once the relative alignment of the pinhole arrays in the conjugate planes had been well established, wavefront measurement at 35 field points required about 6 h to perform. The individual-frame exposure times varied from 20 to 30 s depending on the electron current in the synchrotron storage ring.

B. Wavefront improvement through at-wavelength alignment

Figure 2 shows the rms wavefront-error magnitude at 35 points across the field of view, based on reconstructions from a 37 term Zernike polynomial fit. The measurement-dependent *piston*, *tilt*, and *defocus* terms have been subtracted from the reconstructions. Measurement uncertainty for the individual rms wavefront error magnitudes is below 0.1 nm for all measurements. Uncertainty magnitudes for the individual Zernike polynomial coefficients, based on repeated uncorrelated measurements and separate system accuracy characterizations, are estimated to be below 0.1 nm. Values between the measured points are determined by two-dimensional interpolation.

Each of the adjustments performed during the alignment iterations was successful in reducing the field-weighted wavefront error magnitude. Within each iteration, adjustments were made to the tilt and longitudinal positions of the mirrors, and to the positions of the conjugate planes—all other degrees of freedom were held fixed. Owing to the limitations of rigid body motion for aberration compensation, these adjustments primarily affected the wavefront astigmatism, and to a much lesser degree, coma. Other, higher-ordered wavefront aberrations, such as spherical aberration and trifoil, or triangular astigmatism, were largely unaffected by the adjustments. After two alignment adjustments, the field-weighted rms wavefront error was reduced to the point where no further improvements could be made.

Figure 3 shows the rms astigmatism, coma, spherical aberration, and trifoil magnitudes within each of the alignment iterations. Notice the significant reduction in astigmatism from the first to the final measurements; the other aberration components remain nearly constant. Once again, values between the measured field point positions are interpolated. The set of 35 wavefront phase maps recorded after the final alignment iteration is shown in Fig. 4. Figure 4 wavefronts on the left are based on 37 term Zernike polynomial reconstructions; Fig. 4 wavefronts on the right are generated from the same data yet contain the available midspatial-frequency content measured by the PS/PDI.

IV. CONCLUSION

In addition to the efficacy of the alignment method, the measurements reveal both the stability of the optical system's housing and the high degree of repeatability of the interferometer. Series of wavefront measurements recorded across the field of view were used to reduce the field-weighted rms wavefront error in two iterations. Small adjustments in the mirror positions and tilt angles were able to significantly reduce the wavefront astigmatism until no further improvement was possible. While the system measure-

ments were performed over a six week period, a single measurement series could be performed in approximately 6 h.

Detailed comparison of the EUV and visible-light wavefront measurements of this optical system is the subject of a separate article in these proceedings.[23] The comparisons show very good wavefront agreement, particularly for the midspatial-frequency wavefront features, with some as-yet unresolved small discrepancies in the low-spatial-frequency wavefront components.

ACKNOWLEDGMENTS

The authors are grateful for the hard work and contributions of the CXRO engineers and staff, including Keith Jackson, Kevin Bradley, Brian Hoef, David Richardson, Farhad Salmassi, M. Gideon Jones, Nord Andreson, Lon Amerman, René Delano, Matt Bjork, James Comins, Douglas Lahti, and Kevin Geary. They are also indebted to Dino Ciarlo for wafer processing. Technical assistance with the POB alignment was provided by Nhan Nguyen. This research has been supported by the Extreme Ultraviolet Limited Liability Company (EUV LLC), the DARPA Advanced Lithography Program, and by the Office of Basic Energy Sciences of the U.S. Department of Energy.

[1]D. A. Tichenor *et al.*, Proc. SPIE **2194**, 95 (1994).
[2]G. F. Cardinale, C. C. Henderson, J. E. M. Goldsmith, P. J. S. Mangat, J. Cobb, and S. D. Hector, J. Vac. Sci. Technol. B **17**, 2970 (1999).
[3]K. Sugusaki, T. Oshino, K. Murakami, T. Watanabe, H. Kinoshita, A. Miyafuji, S. Irie, and S. Sirayone, Proc. SPIE **3997**, 751 (2000).
[4]K. A. Goldberg, P. Naulleau, S. H. Lee, C. Chang, C. Bresloff, R. Gaughan, H. N. Chapman, J. Goldsmith, and J. Bokor, Proc. SPIE **3676**, 635 (1999).
[5]K. A. Goldberg, P. Naulleau, and J. Bokor, J. Vac. Sci. Technol. B **17**, 2982 (1999).
[6]J. S. Taylor, G. E. Sommargren, D. W. Sweeney, and R. M. Hudyma, Proc. SPIE **3331**, 580 (1998).
[7]J. H. Underwood and E. M. Gullikson, Proc. SPIE **3331**, 52 (1998).
[8]C. Montcalm, R. F. Grabner, R. M. Hudyma, M. A. Schmidt, E. Spiller, C. C. Walton, M. Wedowski, and J. A. Folta, Proc. SPIE **3767**, 210 (1999).
[9]C. Montcalm, S. Bajt, P. B. Mirkirimi, E. Spiller, F. J. Weber, and J. A. Folta, Proc. SPIE **3331**, 42 (1998).
[10]P. Naulleau, K. A. Goldberg, E. M. Gullikson, and J. Bokor, J. Vac. Sci. Technol. B **17**, 2987 (1999).
[11]E. Tejnil, K. A. Goldberg, and J. Bokor, Appl. Opt. **37**, 8021 (1998).
[12]D. T. Attwood *et al.*, IEEE J. Quantum Electron. **35**, 709 (1999).
[13]P. Naulleau, K. A. Goldberg, S. Lee, C. Chang, C. Bresloff, P. Batson, D. Attwood, and J. Bokor, Proc. SPIE **3331**, 114 (1998).
[14]P. P. Naulleau, K. A. Goldberg, S. H. Lee, C. Chang, D. Attwood, and J. Bokor, Appl. Opt. **38**, 7252 (1999).
[15]K. A. Goldberg, P. Naulleau, and J. Bokor, J. Vac. Sci. Technol. B **17**, 2982 (1999).
[16]D. A. Tichenor *et al.*, Proc. SPIE **3997**, 48 (2000).
[17]J. S. Taylor, G. E. Sommargren, D. W. Sweeney, and R. M. Hudyma, Proc. SPIE **3331**, 580 (1998).
[18]H. Medecki, E. Tejnil, K. A. Goldberg, and J. Bokor, Opt. Lett. **21**, 1526 (1996).
[19]H. Medecki, U.S. Patent No. 5 835 217, Nov. 1998.
[20]K. A. Goldberg, P. Naulleau, P. J. Batson, P. Denham, J. Bokor, and H. N. Chapman, Proc. SPIE **3997**, 867 (2000).
[21]E. H. Anderson, V. Boegli, and L. P. Murray, J. Vac. Sci. Technol. B **13**, 2529 (1995).
[22]H. N. Chapman and D. W. Sweeney, Proc. SPIE **3331**, 102 (1998).
[23]H. N. Chapman, K. A. Goldberg, P. Naulleau, R. M. Hudyma, and J. Bokor, J. Vac. Sci. Technol. B, these proceedings.